The Role of Bottom Pressure Torques on the Interior Pathways of North Atlantic Deep Water

PAUL SPENCE

Climate Change Research Centre, University of New South Wales, Sydney, New South Wales, Australia

OLEG A. SAENKO

Canadian Centre for Climate Modelling and Analysis, Environment Canada, Victoria, British Columbia, Canada

WILLEM SIJP AND MATTHEW ENGLAND

Climate Change Research Centre, University of New South Wales, Sydney, New South Wales, Australia

(Manuscript received 16 September 2010, in final form 28 June 2011)

ABSTRACT

Four versions of the same global climate model, one with horizontal resolution of 1.8° × 3.6° and three with 0.2° × 0.4°, are employed to evaluate the role of ocean bottom topography and viscosity on the spatial structure of the deep circulation. This study is motivated by several recent observational studies that find that subsurface floats injected near the western boundary of the Labrador Sea most often do not continuously follow the deep western boundary current (DWBC), in contrast to the traditional view that the deep water formed in the North Atlantic predominantly follows the DWBC. It is found that, with imposed large viscosity values, the model reproduces the traditional view. However, as viscosity is reduced and the model bathymetry resolution increased, much of the North Atlantic Deep Water (NADW) separates from the western boundary and enters the low-latitude Atlantic via interior pathways distinct from the DWBC. It is shown that bottom pressure torques play an important role in maintaining these interior NADW outflows.

1. Introduction

Observed ocean kinetic energy is dominated by mesoscale features (length scales of 10–100 km) (Ducet et al. 2000), with eddy kinetic energy often found to be 100 times larger than the mean (Wunsch 2007). In contrast, the vast majority of global general circulation model (GCM) simulations, particularly those used in paleoclimatic studies and in long-term climate projections, are often limited to coarse horizontal resolutions (i.e., >1°). These GCMs are obliged to parameterize the effects of unresolved flows, placing the burden of proof on modelers to demonstrate that their simulations accurately represent the flow characteristics under consideration. The Intergovernmental Panel on Climate Change (IPCC) Third Assessment Report (TAR) noted considerable debate regarding the adequacy of coarse-resolution ocean models and warned that results reliant on meridional heat transports from ocean models with >1° resolution should be treated cautiously (McAvaney et al. 2001). The Fourth Assessment Report (AR4) further identified the lack of a comprehensive suite of high-resolution global climate simulations as restricting the ability to draw firm conclusions from GCMs (Randall et al. 2007). Mesoscale-resolving ocean models are currently limited by computational constraints requiring nonglobal spatial domains with idealized boundary conditions and/or short integration periods that make it difficult to evaluate deep ocean flows (e.g., Smith et al. 2000; Oschlies 2002; Treguier et al. 2005). They also are commonly run as uncoupled ocean models with specified surface heat and freshwater fluxes, despite the knowledge that small changes in the buoyancy exchange between climate components (e.g.,

Corresponding author address: Paul Spence, Climate Change Research Centre, University of New South Wales, Sydney, NSW 2052, Australia.
E-mail: paul.spence@unsw.edu.au

DOI: 10.1175/2011JPO4584.1

ocean and atmosphere) can have strong impacts on the ocean circulation (Weaver and Hughes 1992).

This study employs a suite of global coupled GCM simulations to explore the gap between coarse and mesoscale-resolving ocean models. The focus is on the Atlantic meridional overturning circulation (AMOC), which is responsible for the majority of poleward ocean heat transport in the Northern Hemisphere (Hall and Byrden 1982). The AMOC is generally considered to consist of an upper and lower limb (Lozier 2010; Wunsch 2002). The upper limb transports warm, saline surface water northward to deep-water formation sites predominately found in the Labrador and Greenland–Iceland–Norwegian (GIN) Seas. The lower limb transports the recently ventilated cold, dense North Atlantic Deep Water (NADW) southward. Among early attempts to model the lower limb of this circulation, the work by Stommel and Arons (1960) is perhaps the most influential. In their theoretical model, a strong deep western boundary current (DWBC) is required to compensate for the sources of dense water formation in high-latitude regions and to close the poleward transport in the interior. Although some of the assumptions made by Stommel and Arons (e.g., flat-bottomed ocean, uniform deep-water upwelling) can be difficult to justify, it was until recently widely thought that the flow of NADW occurs mainly within such a DWBC. Some hydrographic observations, albeit at only a limited number of locations along the western boundary (Talley and McCartney 1982; Molinari et al. 1992; Pickart 1992; Smethie et al. 2000), can be used to support such a view.

More recent observations of subsurface floats injected near the western boundary of the Labrador Sea most often do not continuously follow the DWBC. Instead, the floats are commonly advected into the North Atlantic deep interior before recirculating northward or continuing southward, toward the subtropics and tropics (Lavender et al. 2000; Fischer and Schott 2002; Bower et al. 2009; Lozier 2010). The important role of deep interior flows, suggested in these studies, questions the long-standing concept of the DWBC being the dominant pathway for NADW to enter the low-latitude Atlantic. A dominance of the DWBC pathway over the interior pathway is typically supported by coarse-resolution model simulations, as we shall illustrate. In such models the potential vorticity budget is necessarily distorted by the need to impose large lateral viscosity. In contrast, interior NADW pathways into the subtropics have been attributed to the effects of complex, finescale bathymetry and to eddy-driven recirculations, which are both unresolved in coarse-resolution GCMs.

The aim of this study is to evaluate the roles of horizontal grid resolution, bathymetry, and ocean viscosity on the AMOC, with an emphasis on the equatorward flow of NADW. A 1.8° (latitude) × 3.8° (longitude) resolution simulation is compared to three 0.2° × 0.4° simulations that have varying bathymetry and horizontal viscosity. Increasing grid resolution reduces the dependence on subgrid-scale parameterizations and has been shown to improve many features of the North Atlantic including the representation of boundary currents, heat transports, and kinetic energy (e.g., Bryan 1991; Oschlies 2002; Spence et al. 2008). In addition, there are reasons to think that variations in bottom topography, and the associated bottom pressure torques, play an important role in maintaining the large-scale meridional flows (Wunsch and Roemmich 1985; Hughes 2000; Hughes and Cuevas 2001). In coarse-resolution models, however, a large horizontal viscosity has to be imposed, thereby dampening the kinetic energy of the flow (Bryan et al. 1975; Jochum et al. 2008) and, as we shall demonstrate, suppressing the effect of bottom pressure torques on the structure of deep interior currents. In particular, we find that, while the zonally integrated AMOC of these simulations are striking similar, the zonal structures of the lower branch are markedly different. Specifically, NADW predominately follows a DWBC in the simulations that impose a high value for lateral viscosity. In contrast, interior pathways away from the DWBC become a robust feature of high-resolution simulations once ocean viscosity is reduced and bathymetry is better resolved.

2. Methods

This study uses the University of Victoria Earth System Climate Model (UVic ESCM), which couples a vertically integrated energy–moisture balance atmospheric model, a thermodynamic/dynamic sea ice model, and a land surface model with the Geophysical Fluid Dynamics Laboratory Modular Ocean Model (version 2.2) and is described in detail in Weaver et al. (2001). Control-state winds are prescribed from the National Centers for Environmental Prediction–National Center for Atmospheric Research (NCEP–NCAR) 50-Year Reanalysis (NCEP50) monthly-mean climatology (Kistler et al. 2001). In all experiments, the ocean model has 19 vertical levels and the same vertical diffusivity profile. The vertical resolution is coarse relative to most eddy-resolving models but is comparable to other global eddy-permitting coupled climate models (e.g., Jayne and Marotzke 2002). The barotropic momentum equations are solved by the implicit free-surface formulation of Dukowicz and Smith (1994). Surface freshwater fluxes are converted to fluxes of salt with a constant salt-to-freshwater mass ratio of 3.49×10^{-2}. All models are integrated under orbital,

TABLE 1. Horizontal-resolution parameters and equilibration periods of the simulations. The terms A_M, A_{ISO}, and A_{ITH} are the horizontal, isopycnal, and isopycnal thickness diffusion coefficients, respectively. The no-bath high A_M and high A_M 0.2° × 0.4° simulations were initiated from the equilibrium state of the 1.8° × 3.6° model, whereas the low A_M 0.2° × 0.4° model was initiated from the final control state of the high A_M 0.2° × 0.4° simulation.

Resolution	1.8° × 3.6°	No-bath high A_M 0.2° × 0.4°	High A_M 0.2° × 0.4°	Low A_M 0.2° × 0.4°
A_M (10^8 cm^2 s^{-1})	20	1.5	1.5	0.1
A_{ISO}, A_{ITH} (10^6 cm^2 s^{-1})	4	0.75	0.75	0.75
Equilibration (yr)	3000	50	50	50

atmospheric (CO_2 = 295 ppm), and land surface conditions corresponding to the year 1900.

Three ocean eddy-permitting, global domain models with a horizontal resolution 0.2° × 0.4° are initiated from the interpolated 3000-yr equilibrium state of a 1.8° × 3.6° model (see Table 1). The high-resolution models have grid spacings finer than typical ocean eddy wavelengths (100–200 km) (Stammer 1997) but coarser than the Rossby radius of deformation at high latitudes (Smith et al. 2000; Oschlies 2002). Increasing model resolution permits a reduction in both tracer and momentum dissipation coefficients to more realistic values. The Reynolds grid number stability criterion of Bryan et al. (1975) suggests a reduction of the Laplacian horizontal mixing coefficient for momentum (A_M) by roughly the factor increase in resolution to avoid erroneous computational modes. The high A_M 0.2° × 0.4° simulation follows this criterion, using a fairly large A_M value of 1.5 × 10^8 cm^2 s^{-1} to ensure computational stability. However, the applicability of the Bryan et al. linear criterion to coupled model solutions based on primitive equations is not straightforward (e.g., Jochum et al. 2008). To make the dissipation more scale selective, one possibility is to employ the biharmonic form for lateral viscosity. However, this would require introducing different parameterizations for the different model resolutions, something we try to avoid in this intercomparison study. On the other hand, we would like to make a link with existing high-resolution models, such as the Fine Resolution Antarctic Model (FRAM). The FRAM is a primitive equation numerical model of the Southern Ocean (between 24° and 79°S), which has horizontal resolution of 0.25° × 0.5°. It was initiated with a Laplacian viscosity of 0.02 × 10^8 cm^2 s^{-1} and subsequently switched to biharmonic viscosity to improve computational stability (FRAM Group 1991). Therefore, we also discuss a low A_M 0.2° × 0.4° simulation, wherein the Laplacian viscosity coefficient was decreased to 0.1 × 10^8 cm^2 s^{-1}, which is computationally stable and increases the resolved eddy kinetic energy relative to the high A_M run by roughly a factor of 4 (Spence et al. 2009). [Note that a simulation with Laplacian viscosity as low as in the FRAM (0.02 × 10^8 cm^2 s^{-1}) was initialized, but it was found to be computationally unstable on long time scales.] In particular, averaged around 55°N, the North Atlantic near-surface eddy kinetic energy of the low A_M 0.2° × 0.4° simulation is 82 cm^2 s^{-2}, which is roughly one-third of satellite altimetry estimates (see plate 6 of Wunsch 2007). Note also that the along-isopycnal (A_{ISO}) and the Gent and McWilliams (1990) isopycnal thickness diffusion (A_{ITH}) tracer mixing coefficients are reduced to the same value in all three high-resolution models, roughly following the criterion of Bryan et al. (1975) (see Table 1).

Although the horizontal resolution of each model component (ocean, land, atmosphere, and sea ice) is increased in all the 0.2° × 0.4° simulations, only the high A_M and low A_M 0.2° × 0.4° simulations employ resolution-dependent ocean bathymetry (NGDC 2007) (Fig. 1). We also include a no-bath high A_M 0.2° × 0.4° simulation that employs the same horizontal viscosity as the high A_M 0.2° × 0.4° simulation and the same ocean bathymetry as the 1.8° × 3.6° simulation. This allows us to explicitly separate the influences of increasing grid resolution and finescale bathymetry. The number of landmasses and the shape of coastlines are held fixed to the 1.8° × 3.6° model grid in all high-resolution simulations by placing a minimum 125-m (ocean level 2) depth constraint on new bathymetry features.

The simulations presented here are among the longest integrated ocean eddy-permitting global climate simulations currently available. The no-bath high A_M and high A_M 0.2° × 0.4° simulations were initiated from the equilibrium state of the 1.8° × 3.6° model and equilibrated for an additional 50 years, while the low A_M 0.2° × 0.4° model was initiated from the final control state of the high A_M 0.2° × 0.4° simulation and equilibrated for an additional 50 years. Although these high-resolution models underrepresent oceanic eddy kinetic energy relative to observations, they nonetheless permit an evaluation of the role of model resolution, lateral viscosity, and bathymetry in the deep ocean circulation at a near-equilibrium state. Unless otherwise stated, all results presented in the following sections are determined from 5-yr means taken at the end of the model integration periods.

3. Results

a. Model simulations assessment

We begin with a brief evaluation of the UVic ESCM ability to simulate some key ocean climate components.

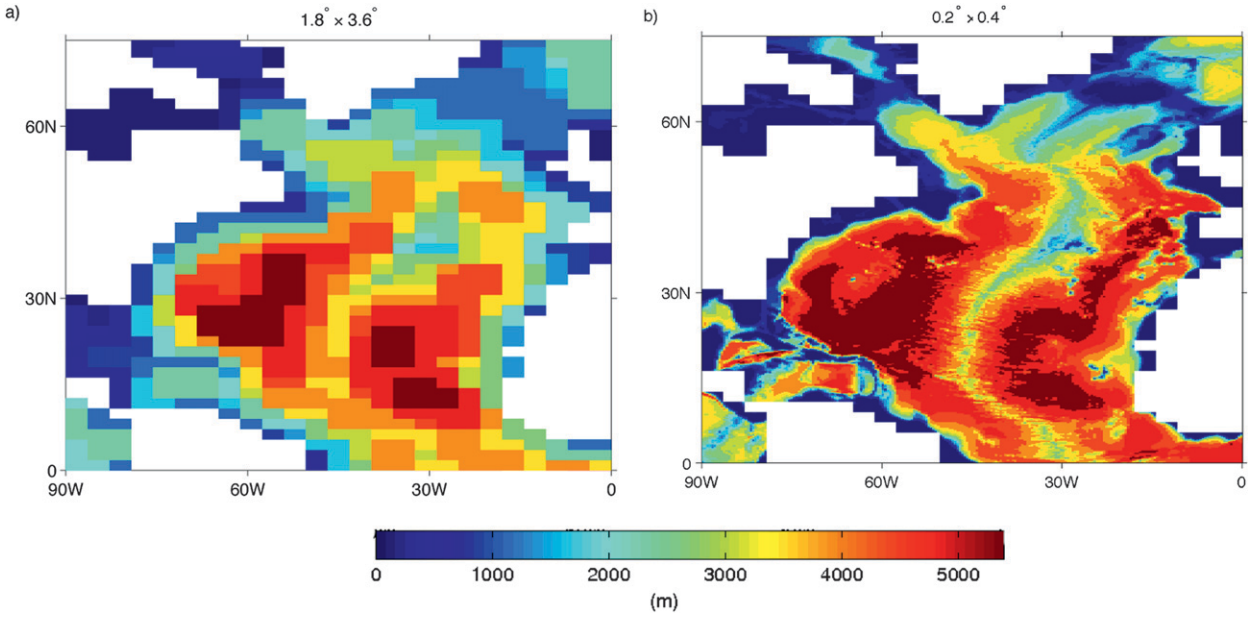

FIG. 1. Low and high resolution North Atlantic bathymetry used by the simulations.

Figure 2 shows the global ocean meridional heat transport produced by the model simulations along with the observational estimate of Ganachaud and Wunsch (2003). Each simulation exhibits poleward transport at all latitudes and an asymmetry across the equator. The simulated transports cover a wide range, sometimes exceeding the uncertainty range provided by Ganachaud and Wunsch (2003), but all values are within the range of other observational estimates (see Fig. 5 of Ganachaud and Wunsch 2003). Roughly ~70% of the total Northern Hemisphere heat transport produced by the model simulations occurs in the North Atlantic, which is also consistent with observed estimates. As shown by previous studies (e.g., Fanning and Weaver 1997; Bryan and Smith 1998; Spence et al. 2008), we find that Northern Hemisphere heat transport is highly sensitive to increasing resolution, with all high-resolution simulations producing substantially more heat transport than the 1.8° × 3.6° case. However, the large-scale Northern Hemisphere heat transport is dominated by the mean circulation, not eddies (Wunsch 1999; Talley 2003).

When A_M is relatively large, the high-resolution bathymetry is found to have little effect on the total Northern Hemisphere heat transport (i.e., compare high A_M 0.2° × 0.4° to no-bath high A_M 0.2° × 0.4°). In contrast, the increased current speeds (discussed below), resulting from lower viscosity, are found to substantially increase the Northern Hemisphere heat transport (i.e., compare high A_M 0.2° × 0.4° to low A_M 0.2° × 0.4°). Although the diffusive heat flux is reduced at high resolution and the eddy heat flux is increased, they consistently remain less than 0.1 PW north of 20°N (not shown). However, locally the heat transport by small-scale and time-varying circulations can be of first-order importance by directly influencing the heat transport via advection and indirectly by modifying the mean flow and surface heat flux budgets, as described by Stammer (1997). Insufficient Northern Hemisphere ocean heat transport is a problem common to coarse-resolution models (e.g., Bryan 1991; Fanning and Weaver 1997; Bryan and Smith 1998; McAvaney et al. 2001). Overall, these results demonstrate that increasing horizontal resolution and lowering ocean viscosity can significantly increase Northern Hemisphere heat transport.

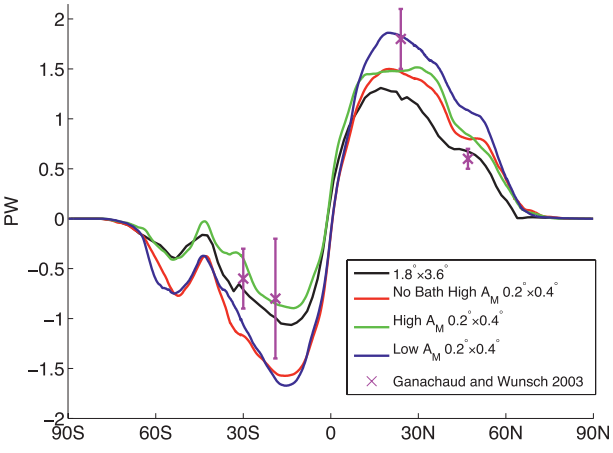

FIG. 2. Total global ocean meridional heat transport (PW) produced by the simulations and observational estimates with uncertainties from Ganachaud and Wunsch (2003).

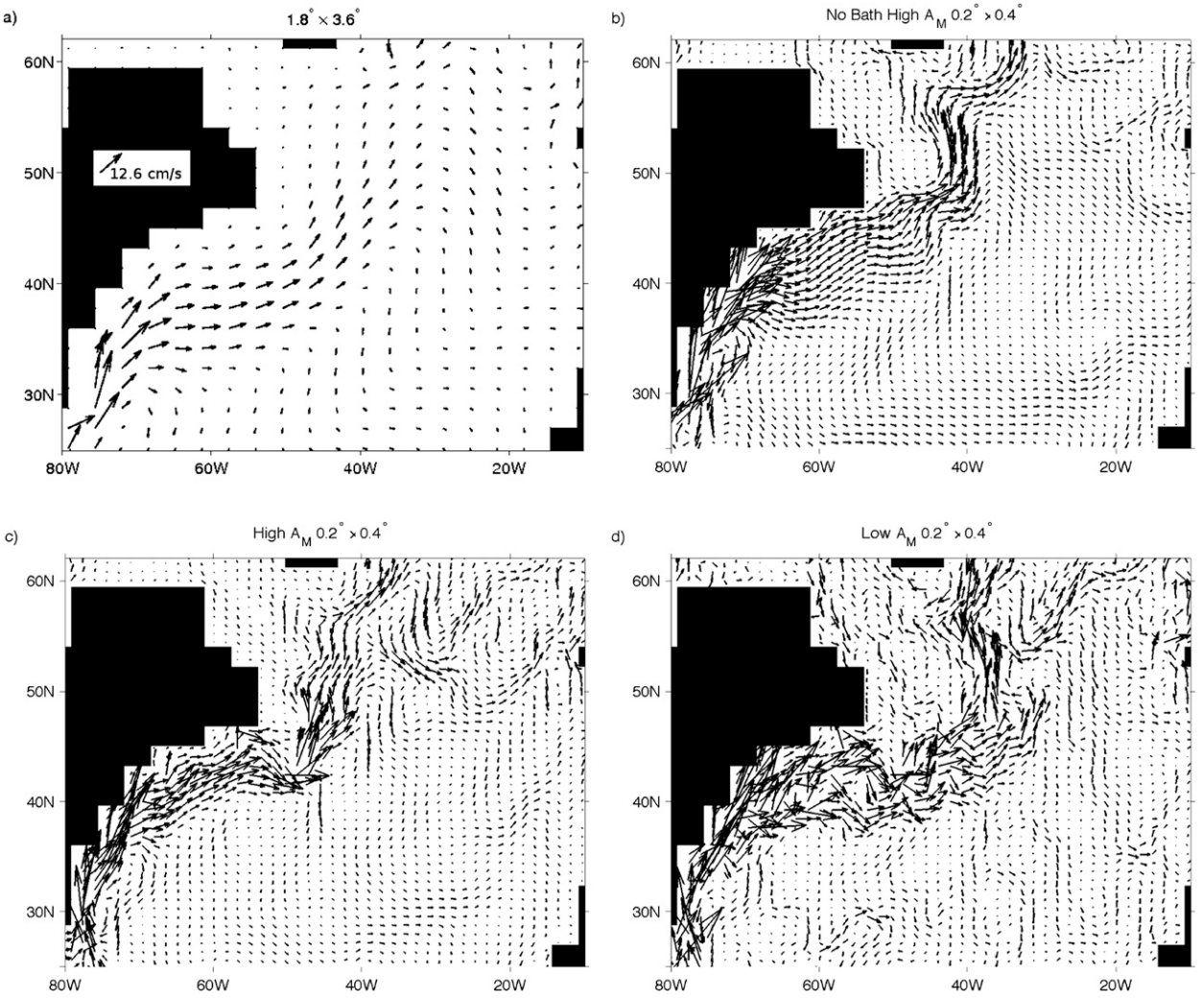

FIG. 3. Annual-mean North Atlantic velocity field at 126-m depth in each simulation. Only vectors at every fourth grid point are plotted for the 0.2° × 0.4° simulations to aid clarity. The velocity fields of all simulations are normalized to the scaling vector in panel (a).

In agreement with previous modeling studies (Smith et al. 2000; Treguier et al. 2005), increased North Atlantic heat transport can be attributed to the improved resolution of the large-scale ocean currents. The simulated maximum near-surface (126-m depth) current speed of the Gulf Stream along 68°W increases from 13 cm s^{-1} at 1.8° × 3.6° to 67 cm s^{-1} in the low A_M 0.2° × 0.4° simulation, with observed estimates in this region of 70 cm s^{-1} (Johns et al. 1995). The maximum near-surface speed of the Labrador Current near 55°W also increases from 4 to 16 cm s^{-1} between the 1.8° × 3.6° and the low A_M 0.2° × 0.4° simulation, with observed values of roughly 30 cm s^{-1} (Flatau et al. 2003). The near-surface velocity field (Fig. 3) confirms that the representation of the Gulf Stream, North Atlantic Current, and Labrador Current are improved with increased grid and bathymetry resolution and decreased viscosity. We also note the presence of recirculations near the Grand Banks in the velocity field of the low A_M 0.2° × 0.4° simulation.

Conservation of potential vorticity q imposes strong constraints on the ocean circulation. Specifically, if frictional and diabatic processes are considered weak, then ocean flow is expected to follow contours of constant q. For large-scale dynamics where the Rossby number is small, the contribution of relative vorticity to q is also small so that q is largely determined by the stretching term; namely, $q = -(f/\rho_0)(\partial\rho/\partial z)$ in which f is the Coriolis parameter, ρ_0 is a reference seawater density, and ρ is the potential density. Earlier modeling work has demonstrated how instabilities in mean currents can drive deep mean flows, particularly near energetic boundary currents (Holland and Lin 1975), and an instability-driven deep flow can be theoretically linked to a homogenized potential vorticity signature (Rhines and Young 1982).

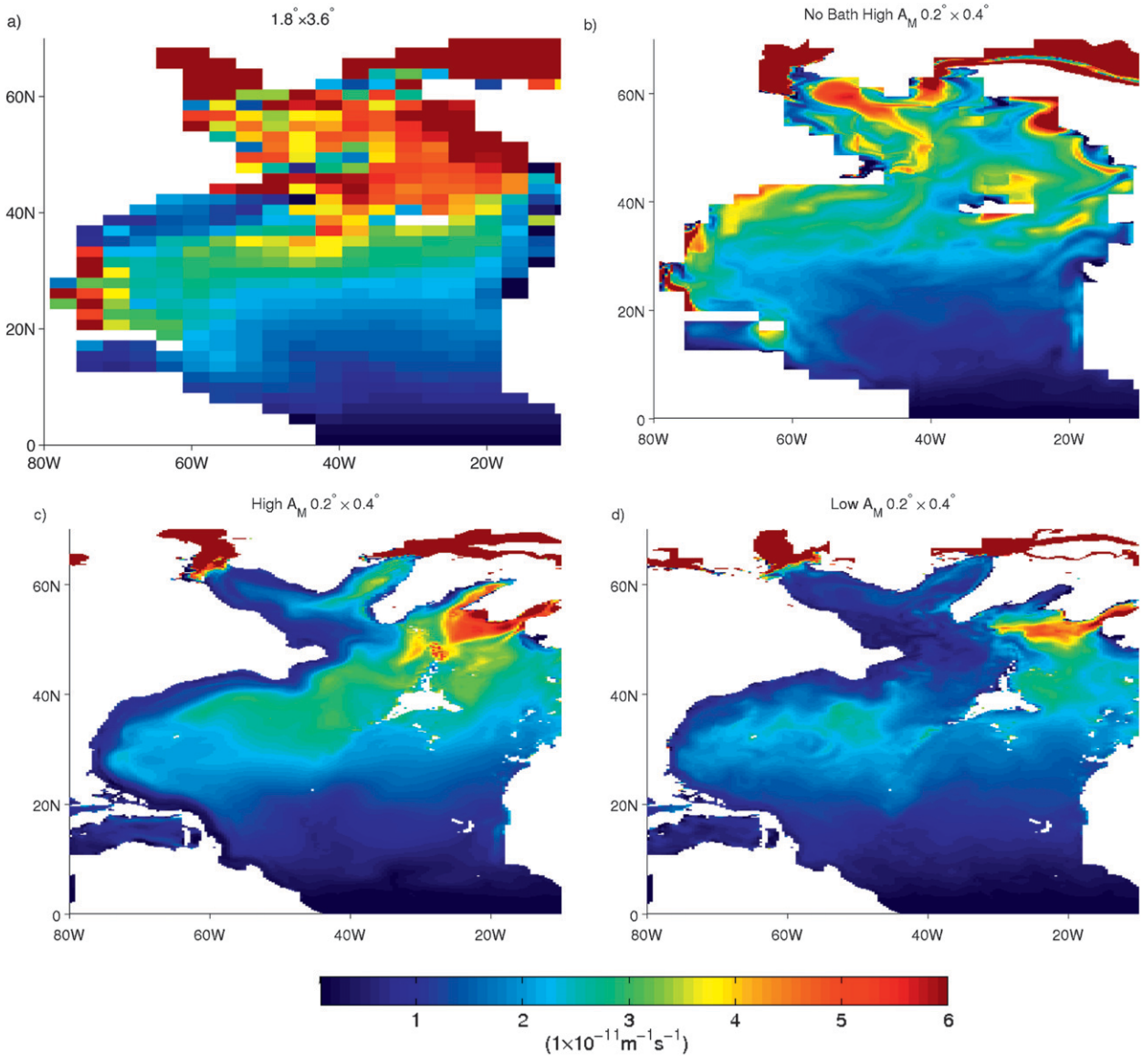

FIG. 4. Annual-mean North Atlantic potential vorticity (m^{-1} s^{-1}), $q = -(f/\rho_0)(\partial\rho/\partial z)$, along the $\sigma_3 = 41.5$ kg m^{-3} isopycnal in each simulation. An observational estimate is excluded towing to the scarcity of deep measurements in Levitus and Boyer (1994) and Levitus et al. (1994).

We evaluate q with potential density referenced to the 3000-m depth (σ_3) as the vertical coordinate to clearly show intermediate depth waters. Figure 4 shows the simulated q field along the $\sigma_3 = 41.5$ kg m^{-3} isopycnal, which corresponds to roughly 2000-m depth south of 50°N in the North Atlantic. Of particular interest is the large pool of nearly homogeneous low q (e.g., the darker blue color) to the west and northwest of the Mid-Atlantic Ridge (MAR) in the low A_M 0.2° × 0.4° simulation; in the model solutions with high A_M, this signature is much less pronounced. Observational (Talley and McCartney 1982; Lozier 1997; Bower and Hunt 2000a,b; Lozier 2010) and eddy-resolving modeling (Getzlaff et al. 2006; Nakamura and Kagimoto 2006) studies discuss a similar homogenized deep q pool. Its presence appears to support the conjecture that instabilities can drive an interior pathway of the low q LSW to the subtropics. We also find eddy kinetic energy in the low A_M 0.2° × 0.4° simulation at 2140-m depth that exceed 30 cm^2 s^{-2} on the northwest of the MAR (Fig. 5). Regardless of the mechanism, the fact that the q simulated by the low A_M simulation hardly varies in this region suggests that little forcing is required to drive deep flow in any direction in this part of the North Atlantic. It may also be indicative of a nonlinear q regime (O'Dwyer

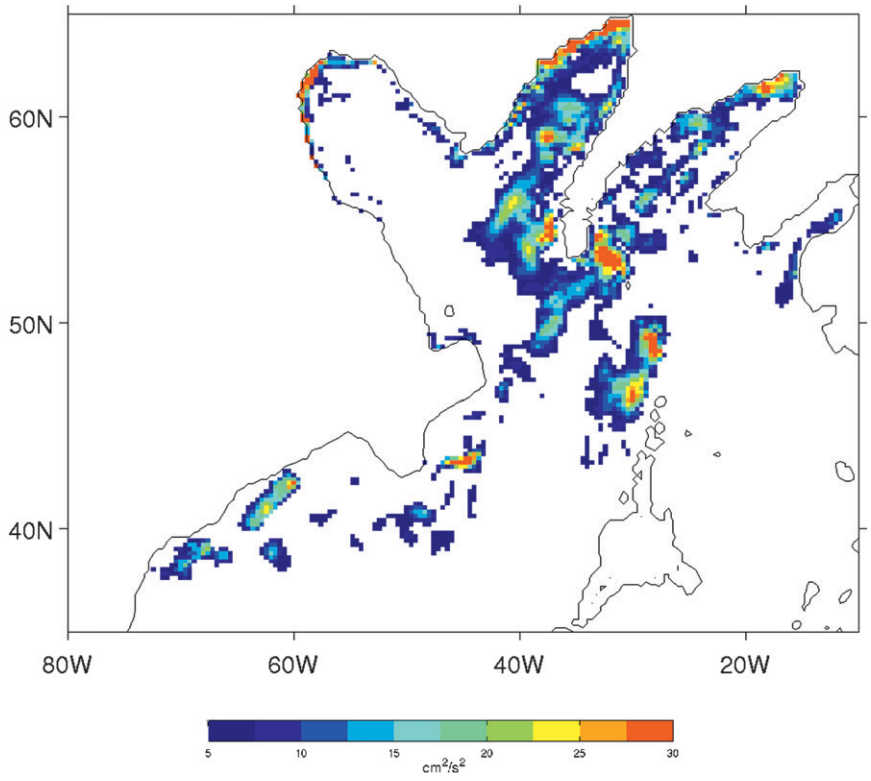

FIG. 5. Eddy kinetic energy ($cm^2\ s^{-2}$) for the low A_M 0.2° × 0.4° simulation at 2140-m depth in the North Atlantic determined from snapshots taken every 5 days for one year.

and Williams 1997; see the appendix), which tends to be suppressed in the coarse-resolution model configuration.

Given the significant differences in the model design and output fields discussed above, the overall similarity in the structure and magnitude of the simulated zonally integrated AMOCs is somewhat surprising (Fig. 6). In particular, all of the simulations have NADW transports ranging from 19 Sv to 23 Sv (Sv $\equiv 10^6\ m^3\ s^{-1}$) that penetrate to roughly 3500-m depth, with a common cell structure. Observational estimates of the present-day NADW volume transport range from 13 Sv to 23 Sv (Ganachaud and Wunsch 2000; Smethie and Fine 2001; Lumpkin and Speer 2003; Talley et al. 2003). We do note that a modest poleward shift in the position of maximum NADW transport from south to north of 40°N can be attributed to the inclusion of high-resolution bathymetry. In general the AMOC in all of the simulations does not penetrate far enough into the GIN Seas, a deficiency that has been attributed to an inability of the model to transport surface waters effectively across the Iceland–Faroes Ridge (Weaver et al. 2001). The cold limb of the AMOC in most models, including this one, is also too shallow compared to observations, due to excess entrainment in the overflows from the Nordic Seas. while the simulated overturning in the North Atlantic is strikingly similar in the four experiments, it should be noted that the dominant pathway for upwelling of NADW has been found to be strongly dependent on grid resolution and horizontal viscosity (see Spence et al. 2009).

b. *Interior versus boundary pathway of NADW*

The equatorward flow of NADW is widely regarded as an important indicator of climate on a wide range of time scales. It has gained much attention, particularly in paleoclimatic studies, where variations in NADW transport are commonly evoked to explain large-scale climate events (Bond et al. 1993; Rahmstorf 2002). As noted in section 1, some hydrographic observations could be interpreted as supporting the widely held view that most NADW enters the subtropics by closely following the deep western boundary pathway. However, recent observations of float trajectories provide evidence that recently ventilated LSW is often advected into the North Atlantic interior when entering the subtropics (Fischer and Schott 2002; Bower et al. 2009; Lozier 2010). Figure 7 shows the magnitude of the North Atlantic velocity field at a depth within the equatorward flowing limb of the AMOC. Observational estimates of the speed of the DWBC between roughly 30° and 55°N range from 5 to 20 cm s^{-1} (Pickart et al. 2005; Bower and Hunt 2000b; Fischer and

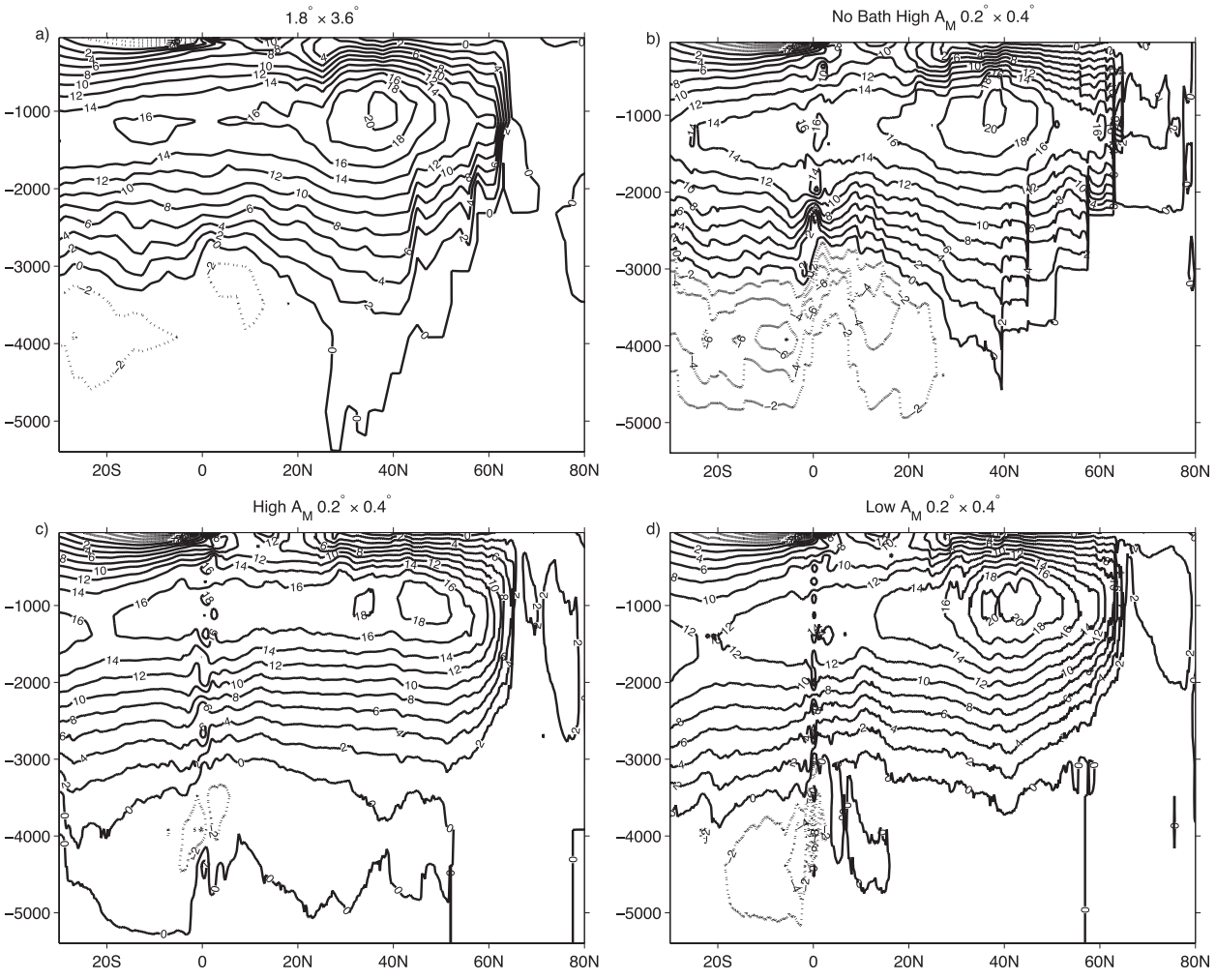

FIG. 6. Simulated annual-mean Atlantic meridional overturning circulation (AMOC) transports (2-Sv contour intervals). Solid (dotted) lines represent clockwise (counterclockwise) flows.

Schott 2002). At coarse resolution the dominant velocity structure is shown to be a weak and broad DWBC that erroneously veers away from the western boundary between roughly 30° and 45°N. An intensified DWBC with speeds within the observed range is found in the no-bath high A_M 0.2° × 0.4° simulation. The DWBC of the high A_M 0.2° × 0.4° simulation also exhibits speeds within the observed range and the flow closely follows the western boundary, but there is also evidence of interior flows, which are predominantly southward (see Fig. 7c), near roughly 50°N. In the low A_M 0.2° × 0.4° simulation, there is a dramatic increase in prevalence of interior flows, which extend into the subtropics by flowing along both western and eastern sides of the MAR, along with a reduced presence of the DWBC between roughly 30° and 50°N, and between 30° and 50°W (see Figs. 7d, 8). Comparable interior flows have been observed in the region between the Grand Banks and the MAR (Rhein et al. 2002; Bower et al. 2009) and on the eastern side of the MAR (Dickson et al. 1985). Overall, we find that, as the simulations become more realistic by lowering viscosity and increasing the grid and bathymetry resolution, the speed and position of the DWBC is improved and interior pathways of NADW outflow into the subtropics become prevalent.

The dependence of NADW pathway partitioning between the interior and western boundary flows on viscosity is further illustrated in Fig. 9, which shows the simulated meridional velocity below 1400 m at 35° and 30°N in the Atlantic. Essentially, a lower horizontal viscosity leads to relatively strong southward interior currents, with deep water entering the low-latitude Atlantic between roughly 30° and 50°W, in addition to the DWBC. The southward interior flows are accompanied by northward velocities in several locations, particularly within 55°–60°W. As can be seen in Fig. 9, none of these interior features is present in

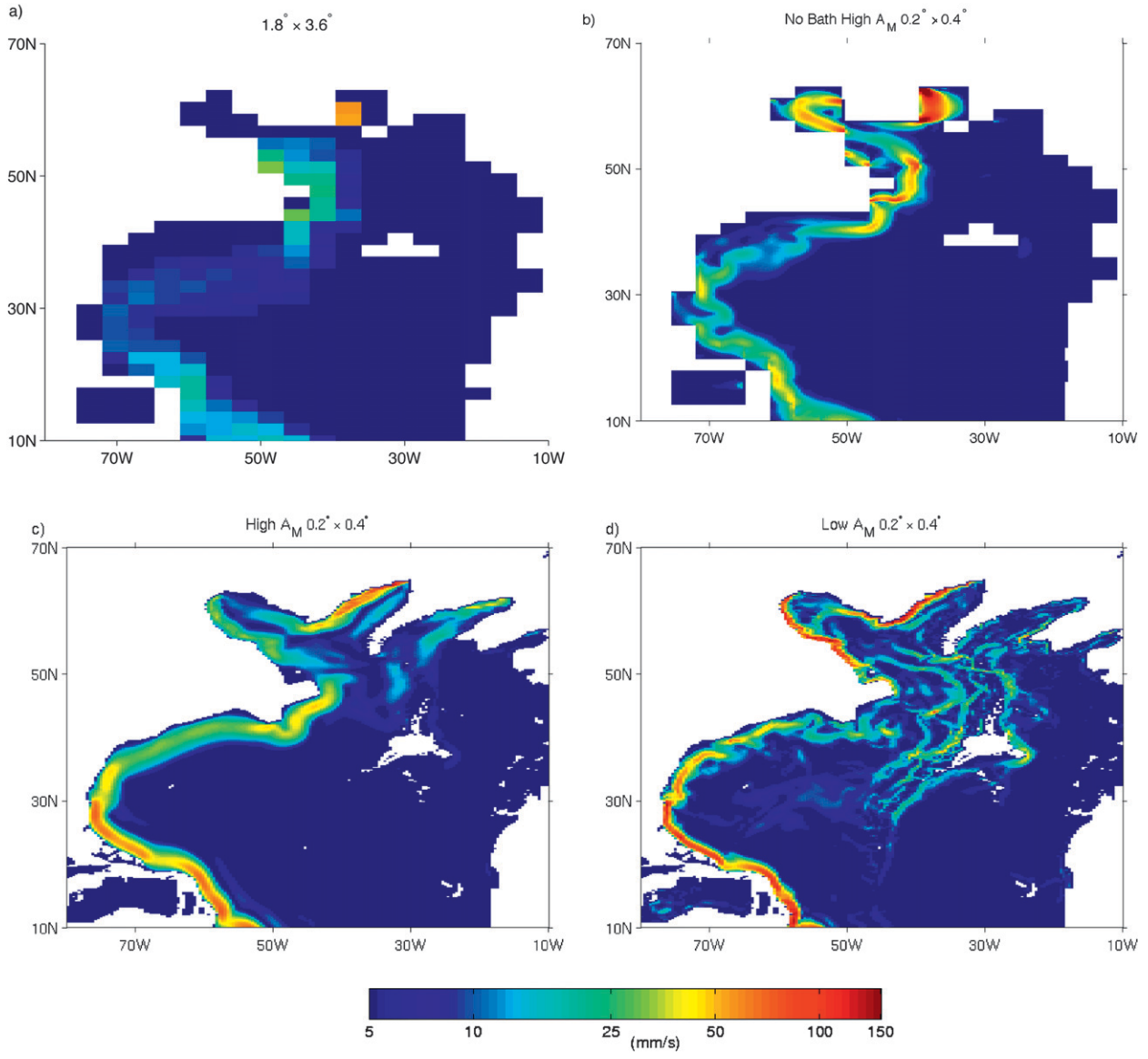

FIG. 7. Simulated annual-mean absolute current speed (mm s^{-1}), $s = \sqrt{u^2 + v^2}$, where u and v are the zonal and meridional velocities, respectively, at 2140-m depth in the North Atlantic. Speeds are shown on a logarithmic scale. Note that the predominant meridional direction at this depth is southward.

the model simulation employing higher viscosity (i.e., with the value of ocean viscosity comparable to those typically imposed in coarse-resolution climate simulations).

The corresponding meridional transport, integrated from the eastern boundary and below 1500-m depth, that is, $V(x) = \int_x^{\text{east}} \int_{-D}^{-1500\text{m}} v(x, z)\, dz\, dx$, is shown in Fig. 10. In the coarse-resolution simulation, nearly all of the transport is found in a broad DWBC beginning at 35°N, around 40°W, and at 30°N, around 60°W. [Recall that the DWBC of this model does not follow the continental margin at 35°N; rather, it extends into the ocean interior (Fig. 7)]. Cross sections similar to that of the coarse-resolution simulation are found for the no-bath high A_M and high A_M 0.2° × 0.4° simulations, with the primary difference being that the DWBC is much better constrained to the western boundary as both the grid and bathymetry resolution are increased. DWBC transport is shown to also be a strong feature of the low A_M 0.2° × 0.4° simulation west of roughly 75°W. However, the low A_M simulation has a substantial amount of lower-limb AMOC transport occurring in the interior, away from the DWBC. Westward of about 40°W the interior southward flow of NADW integrates to a maximum of 15 Sv at 35°N, 50°W and to 8 Sv at 30°N, 50°W, respectively. This southward

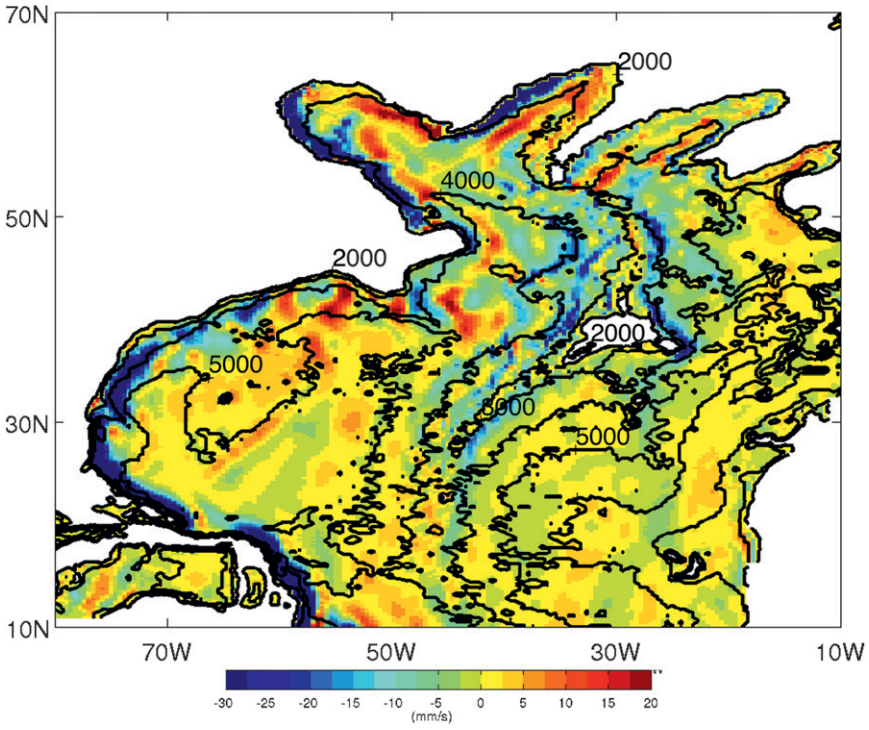

FIG. 8. Annual-mean meridional velocity v (negative values are southward flows) for the low A_M 0.2° × 0.4° simulation at 2140-m depth in the North Atlantic. Black contour lines are isobaths at 1000-m intervals. Dark blue and red corresponds to values of $v < 30$ mm s^{-1} and $v > 20$ mm s^{-1}, respectively.

interior transport is largely offset by northward flows between 50° and 70°W (see also Fig. 9) so that the total transport offshore of the DWBC is about −5 Sv and −1 Sv (negative values being southward) at 35° and 30°N, respectively. Observations of northward flows in this region have been attributed to (i) interior flows of NADW looping south of the Bermuda Rise and then north around the Hatteras Abyssal Plain before joining the DWBC and (ii) an elongated recirculating gyre of NADW (see Fig. 12 of Schmitz and McCartney 1993). In summary, although the zonally integrated AMOC of these simulations is striking similar, the zonal structure can be quite different. This is particularly the case for the low A_M 0.2° × 0.4° simulation, which can be argued to have the most realistic experimental design, in terms of grid resolution, bathymetry, and lateral viscosity.

c. *Dynamical mechanism*

We now seek for a dynamical mechanism to explain the transition from a dominant DWBC to enhanced interior transport of NADW into the subtropics. We begin with the linear vorticity balance,

$$\beta v = f\frac{\partial w}{\partial z}, \tag{1}$$

where $\beta \equiv (\partial f/\partial y)$, v is the meridional velocity, f is the planetary vorticity, and w is the vertical velocity. This balance is a cornerstone of oceanographic theory and it has been widely used to imply deep ocean flow patterns. For example, in the Stommel and Arons (1960) model, Eq. (1) implies, jointly with an imposed upwelling of cold water, weak poleward flow in the deep oceanic interior and strong DWBCs. The Sverdrup balance is the special case when Eq. (1) is vertically integrated between an assumed depth of no motion $z = z_0$ (e.g., 3000 m) and the ocean surface z_1, giving

$$\beta V = fw(z_1) - fw(z_0), \tag{2}$$

where $w(z_1) = w_{\mathrm{Ek}}$ is the Ekman pumping velocity determined by the wind stress curl (Sverdrup 1947). This is equivalent to assuming that the wind stress is the only force acting on the ocean and that bottom topography is unimportant because the motion is confined to the upper ocean. The theoretical basis for these assumptions was strengthened by the success of Munk (1950) in simulating a subtropical gyre with a flat-bottomed, wind-stress-forced barotropic model where lateral viscosity was used to permit closure. However, as noted by Hughes and Cuevas (2001), the assumptions of a depth of no motion

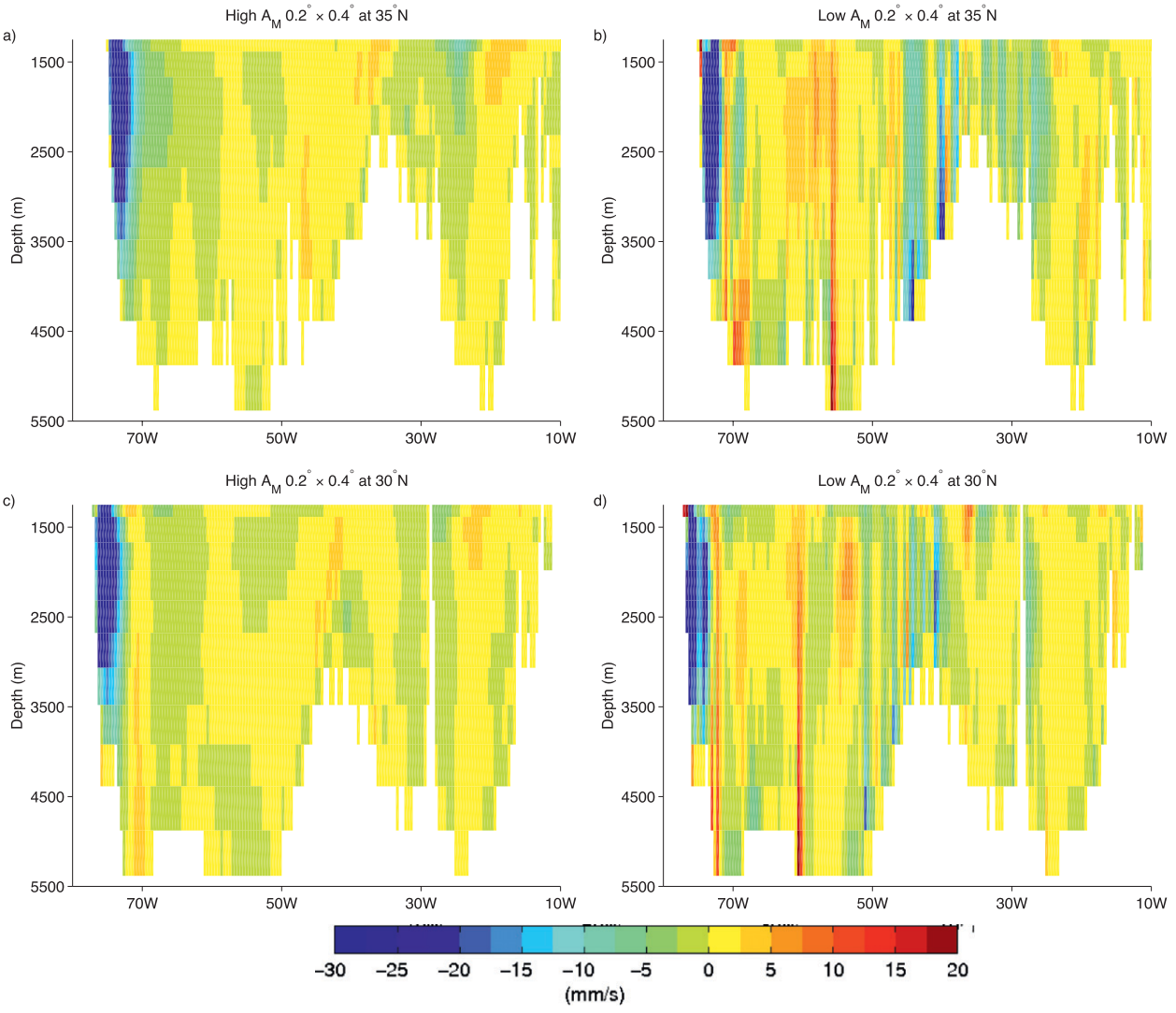

FIG. 9. Simulated annual-mean meridional velocity (mm s^{-1}) below 1400 m at 35° and 30°N in the Atlantic. Velocity is shown on a linear scale. Dark blue corresponds to values of $v < 30$ mm s^{-1}.

and the unimportance of bottom topography were justified only by the reasonable circulation patterns that resulted, not by the underlying physics.

In the observed North Atlantic Ocean, with ample topography and a large-scale convective-driven cell, there is little observational evidence that the subtropical gyre is in Sverdrup balance, even in the relatively quiescent region of the MAR (Wunsch and Roemmich 1985). Hughes and Cuevas (2001) present a convincing theoretical argument, confirmed by an eddy-permitting GCM simulation, showing that, for zonal strips of a few degrees latitude, the dominant balance in the area-integrated barotropic vorticity equation is the wind stress curl and bottom pressure torque, implying that real western boundary currents are largely inviscid—including in the deep ocean. If we remove the level of no motion assumption and, instead, integrate the linear vorticity balance [Eq. (1)] to the seafloor where $z_0 = -D$, then the second term on the right-hand side of Eq. (2) becomes $fw_B = -f\mathbf{u}_B \cdot \nabla D$, where $w_B = w(-D)$ and $\mathbf{u}_B$ is the horizontal velocity at the seafloor, and there is no longer a simple relationship between the meridional transport and the wind stress curl. In this formulation the interior return flow required to balance the western boundary current will be a topographically steered current in which βV is balanced in part by the w_B induced by bottom pressure torques (Hughes and Cuevas 2001).

Indeed, assuming that a representative value for the large-scale horizontal velocity near the bottom $|\mathbf{u}_B|$ is 10^{-2} m s^{-1} and using $|\nabla D| = 10^{-3}$ as a representative value for the magnitude of large-scale bottom topographic slopes, the associated near-bottom vertical velocity $|w_B| = |\mathbf{u}_B||\nabla D|$ can be as large as 10^{-5} m s^{-1}. This is an order of

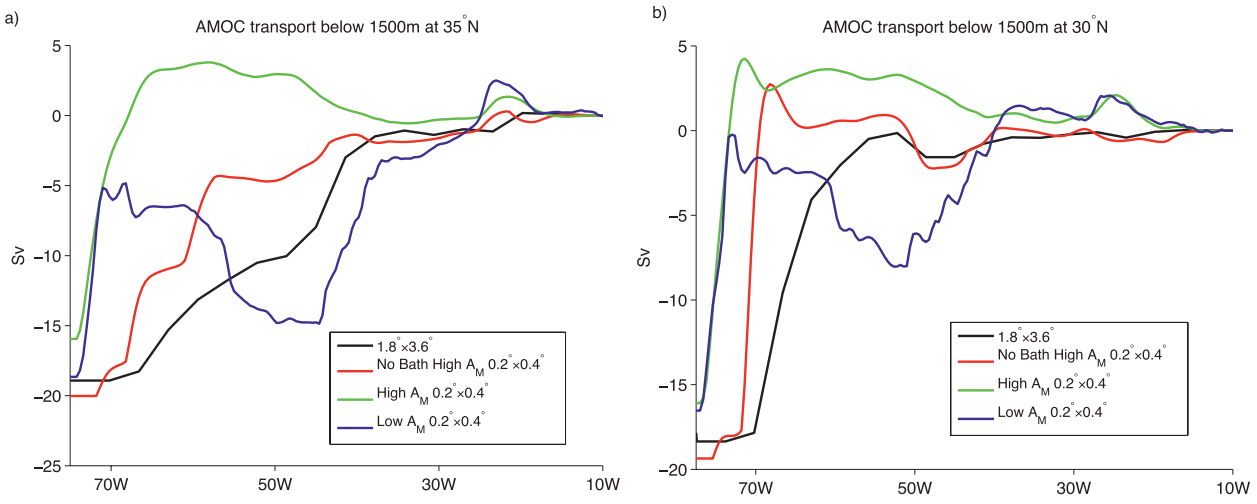

FIG. 10. Simulated annual-mean AMOC transports (Sv) below 1500 m [i.e., $V_{\mathrm{AMOC}<1500\mathrm{m}}(x) = \int_x^{\mathrm{east}} \int_{-D}^{-1500\mathrm{m}} v(x,z)\,dz\,dx$] at 30° and 35°N as a function of longitude. The zonal integral is calculated westward from the eastern boundary of the North Atlantic.

magnitude larger than typical values of surface Ekman pumping. It is also much larger than typical values of mixing-driven upwelling (assuming for the latter a vertical diffusivity of 10^{-4} m^2 s^{-1} acting over a corresponding vertical scale of 10^3 m). Although the above estimate for $|w_B|$ is biased toward its upper limit (since the cross-slope component of $\mathbf{u}_B$ is likely to be generally smaller than $|\mathbf{u}_B|$), it does suggest that the effect of bottom pressure torques can be very important.

Figure 11 shows the bottom pressure torque $\rho_0 f w_B$ for the coarse-resolution simulation along with the high A_M and low A_M 0.2° × 0.4° simulations. Note that w_B is taken as the vertical velocity through the top of those grid cells that are located directly above the seafloor. Figure 11 is dominated by large positive and negative values on small length scales. As noted by Hughes and Cuevas (2001), this can be attributed to the large spatial gradients in bottom stress. This effect can be exacerbated by artificially large nonlinear and viscous forces generated by coarse vertical resolution of bottom topography, especially near large seafloor terraces. It is for this reason that we exclude the no-bath high A_M 0.2° × 0.4° simulation from the figure. A comparison between Fig. 11 and Fig. 4d of Hughes and Cuevas (2001), noting that their GCM has 36 vertical levels, confirms that $\rho_0 f w_B$ provides a reasonable proxy of bottom pressure torque in the model.

For the coarse-resolution model, Fig. 11a shows bottom pressure torque signatures in the subpolar region, but they become much weaker in the subtropics. In the high A_M 0.2° × 0.4° simulation, intense bottom pressure torques become evident throughout the subpolar region and along the western boundary of North America (Fig. 11b). In the low A_M 0.2° × 0.4° case, the signature of bottom pressure torque is further amplified along the western boundary and becomes increasingly evident in the interior of the subtropical gyre near the Mid-Atlantic ridge [with absolute values $O(10^{-6}$ N m$^{-3})$ and with $|w_B| \approx 10^{-5}$ m s^{-1}, which is not uncommon] (Fig. 11c). The rugged bathymetry of the high-resolution simulations leads to noisy bottom pressure torque patterns. Figure 11d presents a smoothed version of the low A_M 0.2° × 0.4° bottom pressure torque field, wherein each grid point is plotted as the mean of the surrounding 3 × 3 gridpoint area of Fig. 11c. The amplified bottom pressure torque signature in the low A_M 0.2° × 0.4° simulation is not surprising because a reduction in horizontal viscosity should result, at least in the zonally and depth-integrated vorticity balance, in the input of vorticity by wind stress curl being largely balanced by bottom pressure torques. Locally, however, one may also expect changes in the advection of planetary vorticity βv, including in the deep ocean. Indeed, even before analyzing this in more detail, we note that the spatial pattern of Figs. 7b,c resembles that of Figs. 11b,c for the high A_M and low A_M simulations. This suggests that bottom pressure torque may play an important role in maintaining the pathways of NADW outflows. The smoothed low A_M 0.2° × 0.4° bottom pressure torque field (Fig. 11d) clarifies a tendency for large, positive torque values between 30° and 50°W to be positively correlated with the southward interior flows of Fig. 8.

We now compare the simulated meridional transport of the AMOC below 1500 m as function of longitude, $V_{\mathrm{AMOC}<1500\mathrm{m}}(x) = \int_x^{\mathrm{east}} \int_{-D}^{-1500\mathrm{m}} v(x,z)\,dz\,dx$, with that predicted by the linear vorticity balance. The corresponding linear vorticity balance estimate, $V = V_1 + V_2$, is determined by solving for $V_1 = f\beta^{-1}\int_x^{\mathrm{east}} w(-1500\,\mathrm{m})\,dx$ and $V_2 = -f\beta^{-1}\int_x^{\mathrm{east}} w_B\,dx$, that is, by zonally integrating $w(-1500$ m) and w_B westward from the eastern

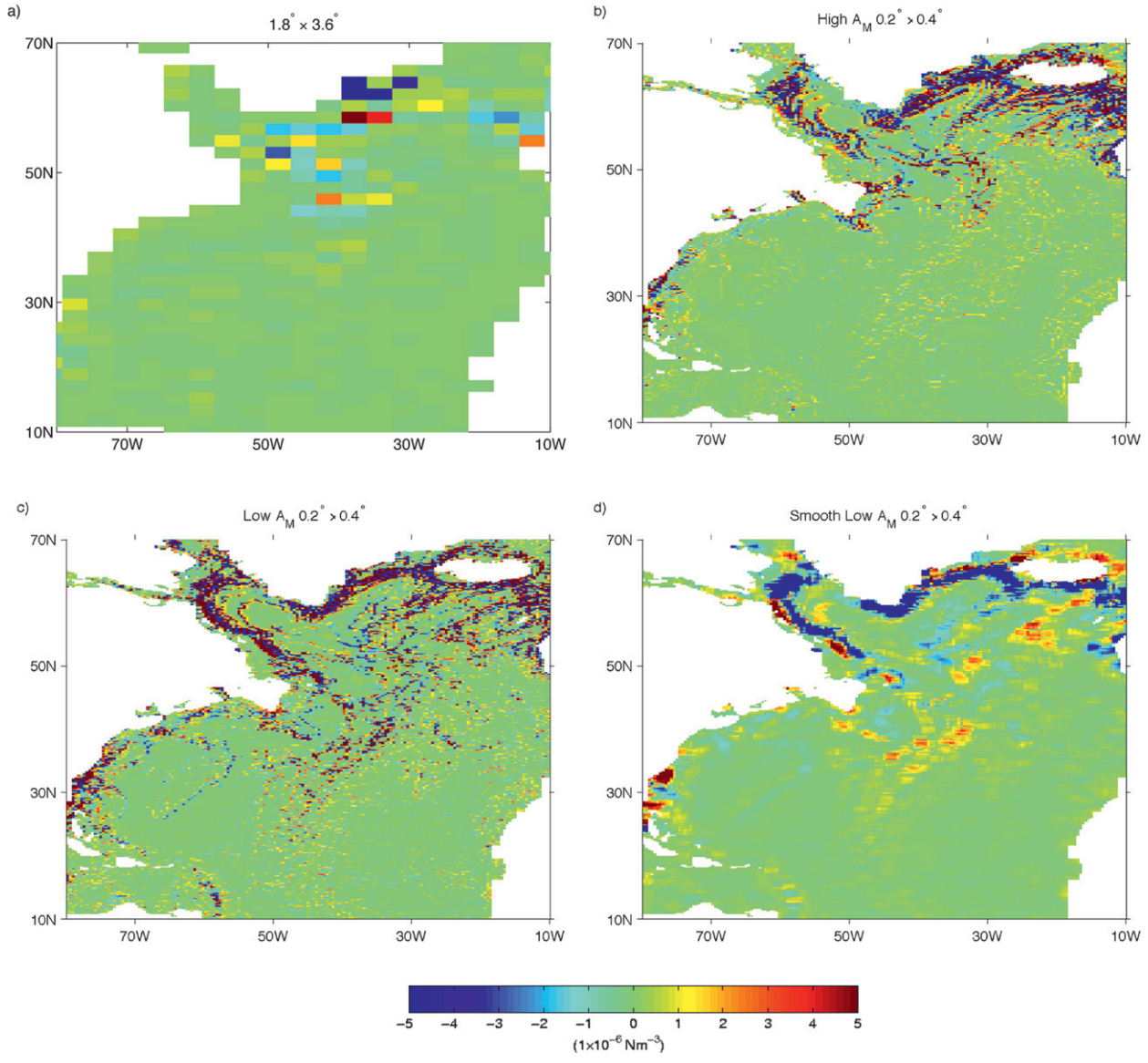

FIG. 11. Annual-mean North Atlantic bottom pressure torque (N m^{-3}) estimated as $\rho_0 f w_B$ in which w_B is the vertical velocity through the top of grid cells located directly above the seafloor, ρ_0 is a reference density, and f is the Coriolis parameter. (d) A smoothed version of (c) via an area-mean filter.

boundary. If the linear vorticity balance holds one would expect $V_{\mathrm{AMOC<1500m}}$ to closely follow V in the interior. At the western boundary, other terms (e.g., nonlinear terms) are likely to upset the linear vorticity balance. In an attempt to filter out what could be considered "noise" in the high-resolution simulations due to nonlinear terms, an average over nine 0.2°-wide zonal bands is taken for both V_1 and V_2. It should also be remembered that these are approximate calculations, in that the vertical velocity is only available at the bottom or at the top of a grid box in the model. Therefore, some of the meridional flow (e.g., very near the bottom) could be missing and the associated error(s) can accumulate upon integration. The results at 30°N are shown in Fig. 12, where $V_{\mathrm{AMOC<1500m}}$ is taken directly from Fig. 10. Outside of the western boundary, V_1 is weak in all of the models, whereas V_2 contributes significantly to the structure of V, which demonstrates the important role of bottom pressure torque in the linear vorticity balance, even when viscosity is large.

The discrepancy between simulated meridional transport $V_{\mathrm{AMOC<1500m}}$ and that predicted by the linear vorticity V is largest for the high A_M run. This can be attributed to strong frictional effects in the presence of topography, which tend to suppress the deep interior meridional flows

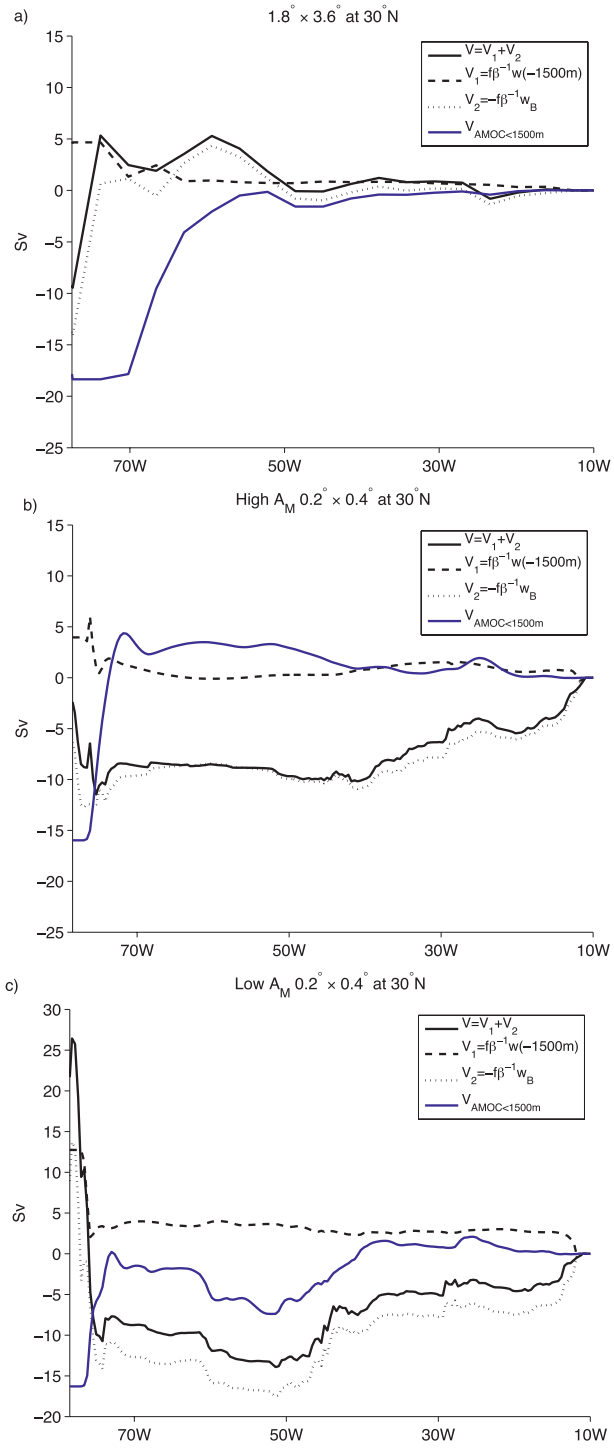

FIG. 12. Comparison of simulated annual-mean AMOC transports below 1500 m at 30°N, as given in Fig. 10, with that predicted by the linear vorticity balance, $V = V_1 + V_2$ with $V_1 = f\beta^{-1}\int_x^{\text{east}} w(-1500\text{ m})\,dx$ and $V_2 = -f\beta^{-1}\int_x^{\text{east}} w_B\,dx$, as a function of longitude. Zonal integrals are calculated westward from the eastern boundary of the Atlantic.

implied by the bottom pressure torque. However, once the friction is reduced in the low A_M case, the discrepancy becomes smaller and V tends to follow $V_{\text{AMOC}<1500\text{m}}$, including reproducing the accumulation of about 7 Sv in the interior, between roughly 40° and 50°W. Essentially all of this transport is due to V_2, demonstrating that bottom pressure torque is playing a central role in maintaining the deep meridional interior flows of the AMOC. The degree to which linear vorticity dynamics holds in the low A_M model depends on latitude, but generally it does provide a first-order description of the large-scale flows in the deep interior.

We propose that, with increasing resolution and decreasing viscosity, bottom pressure torque becomes a key term in the vorticity balance of the deep interior and can account for much of the meridional vorticity advection. Although the spatial distribution of bottom pressure torque is quite noisy given the rugged bathymetry, the connection between the interior NADW flows (Fig. 8) and the bottom pressure torque (Fig. 11c) is illustrated, in an integral sense, in Fig. 12c. It remains unclear if bottom pressure torques cause or result from the deep interior flows (or both); however, one may consider bottom pressure torques as a necessary component for maintaining the interior flows in the deep North Atlantic.

4. Discussion

Assuming sources of deep, dense water in polar regions of the Atlantic and uniform upwelling elsewhere, Stommel and Arons (1960) proposed a highly influential model for circulation in the abyss. Their model, based on Eq. (1), implied weak poleward flow in the deep interior and strong DWBCs. Since then, the assumptions of uniform upwelling and continuous DWBCs have been questioned. In particular, microstructure measurements (e.g., Polzin et al. 1997) and tracer release experiments (e.g., Ledwell et al. 2000) have demonstrated that the diapycnal mixing driving the deep-water upwelling is far from being uniform. Furthermore, several recent studies find that subsurface floats injected near the western boundary of the Labrador Sea most often do not continuously follow the DWBC; instead, the floats are usually advected into the North Atlantic deep interior, with a portion of them following interior pathways toward the subtropics and tropics (Lavender et al. 2000; Fischer and Schott 2002; Bower et al. 2009; Lozier 2010). In addition, arguments have been presented suggesting that bottom topography, through the bottom pressure torque, can strongly modify large-scale meridional flows (Wunsch and Roemmich 1985; Hughes 2000; Hughes and Cuevas 2001).

Here we tried to demonstrate that models imposing high viscosity in the ocean, which is typical of those limited

to coarse horizontal resolutions (i.e., >1°), are likely to have difficulty in simulating the observed interior pathways of deep-water flow toward the low-latitude Atlantic. Instead, most NADW in such models tends to follow the DWBC. In contrast, high-resolution simulations, wherein the ocean's viscosity can be greatly reduced, are capable of producing interior pathways of NADW toward the subtropics that are, in many ways, not unlike those observed. These results may have important implications for climate simulations, including those dealing with climate changes in the past, as well as those used to project future climate. Some of these implications within a fully coupled model, albeit with a relatively coarse horizontal resolution in the ocean, have been discussed recently by Zhang (2010).

Acknowledgments. We are grateful for the support of Andrew Weaver and the University of Victoria Climate Lab. Special thanks to Marc d'Orgeville and Laura Ciasto of the University of New South Wales for their helpful comments. Infrastructure support from the University of Victoria and the University of New South Wales is also acknowledged. This study was supported by the Australian Research Council. We graciously thank the anonymous referees for their insightful comments.

APPENDIX

Uniformity of Deep-Water Potential Vorticity

For a layer of fluid with thickness h, the large-scale potential vorticity is

$$q = \frac{f}{h}. \tag{A1}$$

In the absence of strong forcing and dissipation in the deep ocean, such as those that may arise due to interfacial friction or diapycnal fluxes, it is expected that

$$\mathbf{u} \cdot \nabla q = 0 \tag{A2}$$

or

$$v\beta = \frac{f}{h}\mathbf{u} \cdot \nabla h, \tag{A3}$$

where $\mathbf{u}(u, v)$ is the horizontal velocity vector. Taking the ratio of these terms gives

$$\frac{h^{-1} f \mathbf{u} \cdot \nabla h}{v\beta} \sim \frac{h^{-1}\Delta h}{f^{-1}\Delta f}. \tag{A4}$$

As discussed in O'Dwyer and Williams (1997), in the nonlinear regime, that is, where $|(\Delta h/h)(\Delta f/f)| \sim 1$, it is expected that q is uniform over the large scale in deep waters.

REFERENCES

Bond, G., W. Broecker, S. Johnsen, J. McManus, L. Labeyrie, J. Jouzel, and G. Bonani, 1993: Correlations between climate records from North Atlantic sediments and Greenland ice. *Nature,* **365,** 143–147.

Bower, A., and H. Hunt, 2000a: Lagrangian observations of the deep western boundary current in the North Atlantic Ocean. Part I: Large-scale pathways and spreading rates. *J. Phys. Oceanogr.,* **30,** 764–783.

——, and ——, 2000b: Lagrangian observations of the deep western boundary current in the North Atlantic Ocean. Part II: The Gulf Stream–deep western boundary current crossover. *J. Phys. Oceanogr.,* **30,** 784–804.

——, M. Lozier, S. Gary, and C. Böning, 2009: Interior pathways of the North Atlantic meridional overturning circulation. *Nature,* **459,** 243–248.

Bryan, F., and R. Smith, 1998: Modelling the North Atlantic circulation: From eddy-resolving to eddy-permitting. *International WOCE Newsletter,* No. 33, WOCE International Project Office, Southampton, United Kingdom, 12–14.

Bryan, K., 1991: Poleward heat transport in the ocean. *Tellus,* **43,** 104–115.

——, S. Manabe, and C. Pacanowski, 1975: A global ocean-atmosphere climate model. Part II. The oceanic circulation. *J. Phys. Oceanogr.,* **5,** 30–46.

Dickson, R., W. Gould, and T. J. Müeller, and C. Maillard, 1985: Estimates of the mean circulation in the deep (>2,000 m) layer of the eastern North Atlantic. *Prog. Oceanogr.,* **14,** 103–127.

Ducet, N., P. L. Traon, and G. Reverdin, 2000: Global high-resolution mapping of ocean circulation from TOPEX/Poseidon and ERS-1 and -2. *J. Geophys. Res.,* **105,** 477–498.

Dukowicz, J., and R. Smith, 1994: Implicit free-surface method for the Bryan-Cox-Semtner ocean model. *J. Geophys. Res.,* **99** (C4), 7991–8014.

Fanning, A. F., and A. J. Weaver, 1997: A horizontal resolution and parameter sensitivity study of heat transport in an idealized coupled climate model. *J. Climate,* **10,** 2469–2478.

Fischer, J., and F. A. Schott, 2002: Labrador Sea Water tracked by profiling floats—From the boundary current into the open North Atlantic. *J. Phys. Oceanogr.,* **32,** 573–584.

Flatau, M., L. Talley, and P. Niiler, 2003: The North Atlantic Oscillation, surface current velocities and SST changes in the subpolar North Atlantic. *J. Climate,* **16,** 2355–2369.

FRAM Group, 1991: An eddy-resolving model of the Southern Ocean. *Eos, Trans. Amer. Geophys. Union,* **72,** 169–174.

Ganachaud, A., and C. Wunsch, 2000: Improved estimates of global ocean circulation, heat transport and mixing from hydrographic data. *Nature,* **408,** 453–457.

——, and ——, 2003: Large-scale ocean heat and freshwater transports during the World Ocean Circulation Experiment. *J. Climate,* **16,** 696–705.

Gent, P., and J. McWilliams, 1990: Isopycnal mixing in ocean circulation models. *J. Phys. Oceanogr.,* **20,** 150–155.

Getzlaff, K., C. W. Böning, and J. Deng, 2006: Lagrangian perspectives of deep water export from the subpolar North Atlantic. *Geophys. Res. Lett.,* **33,** L21S08, doi:10.1029/2006GL026470.

Hall, M., and H. Byrden, 1982: Direct estimates and mechanisms of ocean heat transport. *Deep-Sea Res.,* **29,** 339–359.

Holland, W., and L. Lin, 1975: On the origin of mesoscale eddies and their contribution to the general circulation of the ocean. I. A preliminary numerical experiment. *J. Phys. Oceanogr.,* **5,** 642–657.

Hughes, C., 2000: A theoretical reason to expect inviscid western boundary currents in realistic oceans. *Ocean Modell.,* **2,** 73–83.
——, and B. Cuevas, 2001: Why western boundary currents in realistic oceans are inviscid: A link between form stress and bottom pressure torques. *J. Phys. Oceanogr.,* **31,** 2871–2885.
Jayne, S., and J. Marotzke, 2002: The oceanic eddy heat transport. *J. Phys. Oceanogr.,* **32,** 3328–3345.
Jochum, M., G. Danabasoglu, M. Holland, Y.-O. Kwon, and W. G. Large, 2008: Ocean viscosity and climate. *J. Geophys. Res.,* **113,** C06017, doi:10.1029/2007JC004515.
Johns, W. E., T. J. Shay, J. M. Bane, and D. R. Watts, 1995: Gulf Stream structure, transport, and recirculation near 68°W. *J. Geophys. Res.,* **100** (C1), 817–838.
Kistler, R., and Coauthors, 2001: The NCEP–NCAR 50-Year Reanalysis: Monthly means CD-ROM and documentation. *Bull. Amer. Meteor. Soc.,* **82,** 247–267.
Lavender, K., R. Davis, and W. Owens, 2000: Mid-depth recirculation observed in the interior Labrador and Irminger seas by direct velocity measurements. *Nature,* **407,** 66–68.
Ledwell, J., E. Montgomery, K. Polzin, L. S. Laurent, R. Schmidt, and J. Toole, 2000: Evidence for enhanced mixing over rough topography in the abyssal ocean. *Nature,* **403,** 179–182.
Levitus, S., and T. P. Boyer, 1994: *Temperature*. Vol. 4, *World Ocean Atlas 1994,* NOAA Atlas NESDIS 4, 117 pp.
——, R. Burgett, and T. P. Boyer, 1994: *Salinity*. Vol. 3, *World Ocean Atlas 1994,* NOAA Atlas NESDIS 3, 99 pp.
Lozier, M., 1997: Evidence for large-scale eddy-driven gyres in the North Atlantic. *Science,* **277,** 361–364.
——, 2010: Deconstructing the conveyor belt. *Science,* **328,** 1507–1511.
Lumpkin, R., and K. Speer, 2003: Large-scale vertical and horizontal circulation in the North Atlantic Ocean. *J. Phys. Oceanogr.,* **33,** 1902–1920.
McAvaney, B. J., and Coauthors, 2001: Model evaluation. *Climate Change 2001: The Scientific Basis,* J. T. Houghton et al., Eds., Cambridge University Press, 471–523.
Molinari, R., R. Fine, and E. Johns, 1992: The deep western boundary current in the tropical North Atlantic. *Deep-Sea Res.,* **39,** 1967–1984.
Munk, W., 1950: On the wind-driven ocean circulation. *J. Meteor.,* **7,** 79–93.
Nakamura, M., and T. Kagimoto, 2006: Potential vorticity and eddy potential enstrophy in the North Atlantic Ocean simulated by a global eddy-resolving model. *Dyn. Atmos. Oceans,* **41,** 28–59.
NGDC, cited 2007: National Geophysical Data Center 5-minute gridded global relief data collection. [Available online at http://www.ngdc.noaa.gov/mgg/fliers/93mgg01.html.]
O'Dwyer, J., and R. G. Williams, 1997: The climatological distribution of potential vorticity over the abyssal ocean. *J. Phys. Oceanogr.,* **27,** 2488–2506.
Oschlies, A., 2002: Improved representation of upper-ocean dynamics and mixed layer depths in a model of the North Atlantic on switching from eddy-permitting to eddy-resolving grid resolution. *J. Phys. Oceanogr.,* **32,** 2277–2298.
Pickart, R., 1992: Water mass components of the North Atlantic deep western boundary current. *Deep-Sea Res.,* **39,** 1553–1572.
——, N. Hogg, and W. M. Smethie Jr., 2005: Determining the strength of the deep western boundary current using the chlorofluoromethane ratio. *J. Phys. Oceanogr.,* **19,** 940–951.
Polzin, K., J. Toole, H. Ledwell, and R. Schmitt, 1997: Spatial variability of turbulent mixing in the abyssal ocean. *Science,* **276,** 93–96.
Rahmstorf, S., 2002: Ocean circulation and climate during the past 120,000 years. *Nature,* **419,** 207–214.
Randall, D. A., and Coauthors, 2007: Climate models and their evaluation. *Climate Change 2007: The Physical Science Basis,* S. Solomon et al., Eds., Cambridge University Press, 589–662.
Rhein, M., and Coauthors, 2002: Labrador Sea Water: Pathways, CFC inventory, and formation rates. *J. Phys. Oceanogr.,* **32,** 648–665.
Rhines, P., and W. Young, 1982: Homogenization of potential vorticity in planetary gyres. *J. Fluid Mech.,* **122,** 347–367.
Schmitz, W., and M. McCartney, 1993: On the North Atlantic circulation. *Rev. Geophys.,* **13,** 29–49.
Smethie, W., and R. Fine, 2001: Rates of North Atlantic Deep Water formation calculated from chlorofluorocarbon inventories. *Deep-Sea Res.,* **48,** 189–215.
——, ——, A. Putzka, and E. Jones, 2000: Tracing the flow of North Atlantic Deep Water using chlorofluorocarbons. *J. Geophys. Res.,* **105** (C6), 14 297–14 324.
Smith, R. D., M. E. Maltrud, F. O. Bryan, and M. W. Hecht, 2000: Numerical simulation of the North Atlantic Ocean at 1/10°. *J. Phys. Oceanogr.,* **30,** 1532–1561.
Spence, P., M. Eby, and A. Weaver, 2008: The sensitivity of the Atlantic meridional overturning circulation to freshwater forcing at eddy-permitting resolutions. *J. Climate,* **21,** 2697–2710.
——, O. Saenko, M. Eby, and A. Weaver, 2009: The Southern Ocean overturning: Parameterized versus permitted eddies. *J. Phys. Oceanogr.,* **39,** 1634–1651.
Stammer, D., 1997: Global characteristics of ocean variability from regional TOPEX/POSEIDON altimeter measurements. *J. Phys. Oceanogr.,* **28,** 1743–1769.
Stommel, H., and A. Arons, 1960: On the abyssal circulation of the world ocean—I. Stationary planetary flow patterns on a sphere. *Deep-Sea Res.,* **6,** 140–154.
Sverdrup, H., 1947: Wind-driven currents in a baroclinic ocean; With application to the equatorial currents in the eastern Pacific. *Proc. Natl. Acad. Sci. USA,* **33,** 318–326.
Talley, L., 2003: Shallow, intermediate, and deep overturning components of the global heat budget. *J. Phys. Oceanogr.,* **33,** 530–560.
——, and M. McCartney, 1982: Distribution and circulation of Labrador Sea Water. *J. Phys. Oceanogr.,* **12,** 1189–1205.
——, J. Reid, and P. Robbins, 2003: Data-based meridional overturning streamfunctions for the global ocean. *J. Climate,* **16,** 3213–3226.
Treguier, A. M., S. Theetten, E. P. Chassignet, T. Penduff, R. Smith, L. Talley, J. O. Beismann, and C. Böning, 2005: The North Atlantic subpolar gyre in four high-resolution models. *J. Phys. Oceanogr.,* **35,** 757–774.
Weaver, A. J., and T. M. Hughes, 1992: Stability and variability of the thermohaline circulation and its link to climate. *Trends in Physical Oceanography,* Research Trends Series, Vol. 1, Council of Scientific Research Integration, 15–70.
——, and Coauthors, 2001: The UVic Earth System Climate Model: Model description, climatology, and applications to past, present and future climates. *Atmos.–Ocean,* **39,** 361–428.
Wunsch, C., 1999: Where do ocean eddy fluxes matter? *J. Geophys. Res.,* **104** (C6), 13 235–13 249.
——, 2002: What is the thermohaline circulation? *Science,* **298,** 1179–1181.
——, 2007: The past and future ocean circulation from a contemporary perspective. *Ocean Circulation: Mechanisms and Impacts, Geophys. Monogr.,* Vol. 173, Amer. Geophys. Union, 53–74.
——, and D. Roemmich, 1985: Is the North Atlantic in Sverdrup balance? *J. Phys. Oceanogr.,* **15,** 1876–1880.
Zhang, R., 2010: Latitudinal dependence of Atlantic meridional overturning circulation (AMOC) variations. *Geophys. Res. Lett.,* **37,** L16703, doi:10.1029/2010GL044474.